Modeling Surface Deformations and Hinging Regions in Reinforced Concrete Bridge Columns

Z. F. Alemdar
The Vocational School, Department of Construction, Yildiz Technical University, Istanbul, TURKEY

A. B. Matamoros & J. Browning
Department of Civil, Env, and Arch. Engineering, University of Kansas, Kansas, USA

15 WCEE
LISBOA 2012

SUMMARY:
Understanding the spread of inelastic deformations at various stages of loading is a particularly difficult problem for bridge structures subjected to multiaxial dynamic loading. A high-resolution model of a bridge column was developed using the computer program ABAQUS and calibrated using the measured displacement field in a column of a bridge system subjected to dynamic biaxial loading in an earthquake simulator. The bridge system was subjected to a succession of test trials with increasing earthquake intensity. Computer simulations were performed of the complete sequence of trials, providing information about the variation in the spread of plasticity with the intensity of loading. The main goal of this study was to investigate changes in the spread of plasticity of the bridge column, quantified in terms of curvature demand along the column height and longitudinal reinforcement strain, associated with the displacement demand at various levels of earthquake intensity.

Keywords: Reinforced concrete bridge column; FE modeling; photogrammetry; frequency domain error

1. INTRODUCTION

Bridge systems are proportioned to maintain inelastic deformations within the columns in order to prevent damage to the superstructure. This constitutes a significantly different design philosophy than used for building structures, in which it is preferred to maintain inelastic deformations in the beams to protect the gravity load resisting system. For this reason accurate characterization of the behavior of bridge columns in the inelastic range of response is important for the development of improved computer models to simulate the response of bridge systems under earthquake loading. Being able to determine the spread of inelastic deformations in reinforced concrete bridge columns is very important to evaluate the performance of bridge systems. High-resolution analysis methods are a valuable tool in this process when bridges are subjected to multiaxial loading, or when the structural components have a complex geometric shape.

A high-resolution model of a bridge column was developed using the computer program ABAQUS (Simulia, 2009) and calibrated to estimate the displacement field that was recorded during the dynamic test of a bridge system under biaxial loading (Alemdar et al., 2011a). The effect of various simulation parameters were investigated (Alemdar et al., 2011a) to determine the goodness-of-fit of the displacement and rotation fields recorded during the dynamic response.

The primary objective of this study was to use the calibrated model to examine the effect of displacement demand on the spread of plasticity of the bridge column by evaluating the curvature demand along the column height and longitudinal reinforcement strain at various levels of earthquake intensity.

2. FINITE ELEMENT MODEL OF THE BRIDGE COLUMN

The reinforced concrete bridge system analyzed in this study was tested at the University of Nevada Reno (UNR) laboratory under a series of uniaxial and biaxial earthquake trials with increasing level of intensity (Nelson et. al., 2007). The test specimen is described in a previous study (Alemdar et. al., 2011b). Two different grids were painted on the surface to monitor the displacements of the columns during the earthquake trials (Fig. 1). The intersections of the thick vertical and horizontal lines in both regions were numbered (Alemdar, 2010) as shown in Fig. 1.
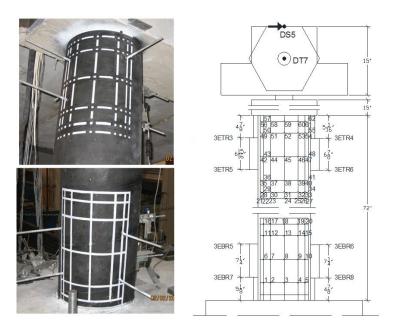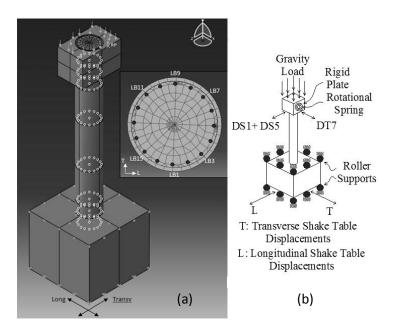

Figure 1. Bottom and top grid systems

Figure 2. Finite Element model and boundary conditions for bridge column:
(a) ABAQUS model and cross-sectional view (RP represents the location of the rotational spring), and (b) sketch illustrating the boundary conditions imposed on the column

A three-dimensional finite element model of the east column of Bent 3 was developed using the computer software ABAQUS (Simulia, 2009). One half of the two-column pier frame system, including the east column, a 23-in. (584-mm) segment of the cap beam, and the footing (Fig. 2a), was

defined in the model. The computer model had a total of 11,750 elements, and the response was analyzed using the implicit static general solution scheme with automatic stabilization available in ABAQUS (Simulia, 2009). A Linux computational cluster with a total of 384 processors was employed to perform the simulations (Alemdar et al., 2011b).

2.1. Material Models

Concrete in the cap beam and the foundation block was modeled as a linear-elastic material because these two structural elements had much larger capacity than the column and experienced no observable damage during the test trials. Concrete in the column and in the connections was defined using the damage plasticity model implemented in ABAQUS (Simulia, 2009). Two different sets of material properties were defined for the concrete in the core and the shell to account for the confinement effects provided by the spiral reinforcement along the column height. The Mander unified stress-strain model under monotonic loading at slow strain rates (Mander, 1984) was taken as the basis of the stress-strain curve in compression for the concrete in the core (Alemdar et. al., 2011b). A maximum strain rate of 0.05 strain per second was adopted in the analysis following recommendations in studies (Wakabayashi 1986, Hosoya et. al. 1997, Mahin et. al. 1972) for reinforced concrete structures subjected to severe earthquake ground motion.

The modulus of rupture of the concrete in tension was taken as $4\sqrt{f'_c}$ (in units of psi). The softening effect of concrete in uniaxial tension, after cracking, was studied to find the best curve for the analysis of the model. Equations proposed by Bhide (1987), Vecchio and Collins (1982), and Collins and Mitchell (1987) were evaluated and the Bhide (1987) tension softening model with a cracking angle of 35° was chosen due to the best performance in the response.

Linear elastic behavior was assumed for the cap beam and foundation block because of the higher stiffness and yield moment in the cap beam (I_g = 4200 in^4, 1.75x10^9 mm^4, M_n^+ = 210 k ft, 284700 kNmm and M_n^- = 180 k ft, 244060 kNmm) than in the column (I_g = 1020 in^4, 4.31x10^8 mm^4, and M_n = 45 k ft, 61015 kNmm). The moment of inertia of the cap beam was varied as a parameter approximately between the cracked (2000 in^4, 8x10^8 mm^4) and gross moments of inertia (4200 in^4, 1.75x10^9 mm^4) of the cross section. The cap beam was also assumed to be infinitely stiff for the additional analyses.

A uniaxial steel model with combined isotropic and kinematic hardening properties was defined to simulate the behavior of the longitudinal steel. A typical stress-strain relationship for ASTM A706 (ASTM 2002) Grade 60 steel was used to describe the isotropic parameters. The strength of the steel was adjusted to account for the effect of strain rate under dynamic loading by using the dynamic magnification factor. Kinematic hardening properties were defined to include cyclic strain softening according to experimental results by Ma et al. (1976). The results from the computational model and the experiment gave a close match for the stress-strain curve of a single element near the center of the steel bar as shown elsewhere (Alemdar et. al., 2011b).

2.2. Finite Element Mesh

The concrete mesh consisted of quadratic brick elements with twenty integration points. Two different segments were defined to model the cap beam. In the first segment, solid elements were used starting at the edge of the cap beam and having a length equal to twice the distance from the edge of the beam to the center of the column (Fig. 2a). In the second segment, a single rotational spring element was used from the end of the first segment to the center of the pier frame. The spring element was rigidly attached to a thin but infinitely stiff layer of transition elements at the center of the right face of the cap beam (Fig. 2b).

The circular column, the cap beam-column, and the column-footing joint regions were modeled using 3D continuum 8-node brick elements with twenty integration points. A reduced-integration scheme was used to decrease the computation time for the analysis. The solid element mesh for the cap beam-

column connection, the column-footing connection, and the circular column was generated taking into account the location of the longitudinal reinforcement (Fig. 2a). A coarse mesh with 4-in. (102-mm) elements was used in the remainder of the two joint regions. 1D 2-node ABAQUS (Simulia, 2009) wire elements were defined to model the longitudinal reinforcement and transverse steel hoops and linked to the edge of the solid elements using embedded constraints. The longitudinal steel had a cross-sectional area of 0.11 in.^{2} (71 mm^2) and transverse hoops had a cross sectional area of 0.029 in.^{2} (18.7 mm^2) evenly distributed every 1.25 in. (32 mm) along the height of the column.

Models with different element sizes in the connections and the column were analyzed to examine the sensitivity of the load-displacement relationship to mesh size. Computed load-displacement relationships under monotonically increasing lateral load for various mesh configurations were compared with (Alemdar et al., 2011b) load-displacement curves based on moment-curvature relationships and the implementation of the modified compression field theory in the computer program Response 2000 (Bentz, 2000). This study showed that the load-deformation curve of the column was sensitive to mesh size (Alemdar et al., 2011b), with smaller mesh sizes resulting in lower column stiffness. The 1-in. (25-mm) mesh model provided the closest match to the force-displacement response prior to yielding computed using the MCFT, with slightly larger displacements near yield that are attributed to the effect of slip of the reinforcement.

The cap beam and the foundation block provided significant confinement to the concrete in the joints because of the embedded longitudinal reinforcement into the cap beam and into the foundation block; therefore, simulations were performed by modeling slip solely through the softening effect of the concrete in tension. This assumption was consistent with the damage pattern observed in the specimens, which experienced negligible damage in the cap beam-to-column and foundation-to-column connections (Alemdar et. al., 2011b).

2.3. Loads and Boundary Conditions

The axial load on the column was calculated based on the tributary area of the column and consisted of an imposed weight of 47.2 kips (210 kN) applied as a uniform pressure at the top surface of the cap beam in the FE model (Fig. 2b). The two lateral components of the earthquake simulator displacement were imposed at the bottom surface of the footing and the recorded displacement components recorded with LVDTs were imposed at the top of the column, in the cap beam (Fig. 2b). Vertical motion was restrained at the top of the footing (Fig. 2b) to simulate the effect of postensioned rods and steel plate washers used to tie the footing to the earthquake simulator.

The ground motions used in the FE model were the scaled components of the Century City Country Club record from the 1994 Northridge, California earthquake. This earthquake record was used in a total of 11 trials, six of them with the bridge subjected to a single component in the longitudinal direction and five trials subjected to both components (Alemdar et. al., 2011b). These 13 trials induced a maximum drift ratio on the column of approximately 4% in the longitudinal direction and 4% in the transverse direction.

2.4. Solution Algorithm

ABAQUS (Simulia, 2009) offers several solution algorithms for problems with unstable nonlinear behavior, based on both implicit and explicit algorithms. An implicit static solution algorithm was chosen because of greater accuracy in estimating the displacement field of the column and using significantly less CPU time than an implicit dynamic solution algorithm.

Although the concrete in the core of the column is well confined, and consequently less prone to cause convergence problems, the concrete in the shell presented a significant challenge. Because the most severe convergence problems are posed by local instabilities in the concrete shell, which have a relatively small effect on the overall response of the column, convergence was achieved without meaningful loss in precision by setting the dissipated energy fraction of the automatic damping

algorithm to 0.002 and relaxing the convergence criteria for the ratio of largest residual to average flux norm and the ratio of largest solution correction to the largest incremental solution value.

2.5. Parameters of the Finite Element Study

The loss of lateral load capacity is generally defined as the point in the load-deflection or moment-deflection relationship corresponding to a reduction of 20% from the maximum moment or shear force recorded in an experiment (Priestley and Park 1987, Paulay and Priestley 1992, Bae 2005, and Berry et. al. 2008). Various researchers have concluded that strain penetration or bar slip (Paulay and Priestley 1992, Berry et. al. 2008, and Mander 1983), axial load demand (Bae 2005, and Watson and Park 1994), and shear span-to-depth ratio (Bae 2005, Sakai and Sheikh 1989, Tanaka and Park 1990, and Bayrak and Sheikh 1997) have a significant effect on the spread of plasticity. Many of these parameters were fixed in the available experimental sets.

3. EVALUATION OF RESULTS FROM THE FINITE ELEMENT MODELS

Figure 3 shows a comparison between displacement values inferred from video images and the optimum finite element model (f_y = 75 ksi, K_g=10^8 lb-in, w_c= 0.8, and w_t=1) at the point of peak displacement demand on the column during Test 4D trial, which had peak ground accelerations of $0.5g$ in transverse direction and $0.6g$ in the longitudinal direction. Direct comparisons of the displacement field at peak response as shown in Fig. 3 are useful measurement to evaluate the accuracy of the FE model at a single point in time.
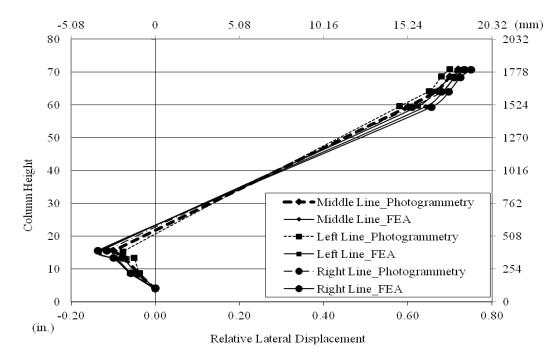

Figure 3. Deformed shape of the bridge column at the maximum drift during Test 4D with f_y=75 ksi (517 MPa), K_g=10^8 lb-in (113x10^5 N-m), w_c=0.8 and w_t=1.0.

The accuracy of the various models over the duration of the Test 4D was assessed by comparing computed displacement and rotation signals at several locations throughout the column with signals recorded with displacement sensors and video images. Comparisons of column rotations between FEA and LVDT results were performed based on values computed about an axis perpendicular to the axis of the cap beam. These rotations were considered to be more important between the two direct measurements recorded with LVDTs due to the relatively large stiffness and strength of the cap beam relative to those of the column, and because the top of the column was essentially unrestrained from rotation about the axis of the cap beam.

Vertical displacement signals from LVDTs were used to interpolate the vertical displacements at grid points and at the surface of the column. Vertical displacement comparisons between FEA and digital imaging signals were performed on the basis of absolute displacement signals, while comparisons between FEA and LVDT signals were performed on the basis of the relative displacements between the two column elevations monitored by the LVDTs.

The Frequency Domain Error index (FDE), developed by Dragovich and Lepage (Dragovich and Lepage 2009), was used to compare measured (or inferred) and computed response quantities. The FDE index uses the Fourier spectra to compare the composition of the two signals, with differences between the Fourier coefficients increasing the value of the error index. The FDE index quantifies the goodness-of-fit of the amplitude and phase of two signals and its value ranges between 0 and 1, where zero indicates a perfect correlation.

The displacement field computed with the finite element model had input data recorded using analog sensors, while the measured displacement field on the surface of the column was inferred from digital video images. Because the two sensors systems performed independently of each other, a direct comparison of the signals obtained with each type of sensor during trial 4D showed the magnitude of the experimental error introduced by differences in the precision of the two sensor systems, which is independent of the modeling assumptions. The best match between the displacements inferred from digital imaging and the earthquake simulator signal yielded a 0.04 FDE amplitude error index and a 0.12 FDE phase error index, for a total error of 0.16. These error values show that an excellent correlation was obtained between the displacements inferred from video images at the base of the column and the earthquake simulator signal.

The lateral displacement signals at the top of the column were compared on the basis of FDE indices. The lateral displacements corresponding to grid Point 58 (Fig. 1), located at near top of the column, were compared with the combined components of the displacement transducers mounted on the bridge deck and the north abutment (DT7, DS1 and DS5 in Fig. 1). The FDE amplitude and phase error indices between the two signals were calculated to be 0.09 and 0.31, respectively, for a total error of 0.40. These computed error values show that the correlation between digital imaging and the LVDT data at the top of the column was not nearly as good as that observed at the bottom of the column between the digital imaging data and FEA signals. The larger discrepancy between sensor readings at the top of the column could be associated with either one of the two sensor systems, flexibilities from anchors and attachment accessories as well as rotation of the cap beam. All of these factors introduce sources of experimental error in the analog sensor readings that do not affect the signal from the earthquake simulator nor the digital imaging.

3.1. As-Built Simulations

A set of simulations was carried out with modeling assumptions intended to represent the as-built characteristics of the frame pier as closely as possible. Material properties were defined based on reported measured values (f'_c = 6.7 and f_y = 64 ksi, 46 and 441 MPa) (Nelson et. al. 2007). The calibration of the finite element model is described in detail elsewhere (Alemdar et. al., 2011b). Rotation signals inferred from FEA and LVDT sensors were compared and the FDE error indices indicated that computed rotation values showed excellent correlations with the experimental data in both hinging regions of the column (Alemdar et. al., 2011b).

As previously mentioned, the bridge was subjected to a sequence of 13 test trials with increasing ground motion amplitude. A simulation of the sequence of the 13 trials was performed using the finite element model to track the change in spread of plasticity as a function of the increase in deformation demand on the column. The displacement history along the transverse direction recorded at the top of the bridge deck is shown in Fig. 4.

The spread of plasticity for each earthquake trial was calculated for the point corresponding to the maximum relative drift demand during the trial. The drift demand was quantified as the resultant of

the longitudinal and transverse components of the drift ratio during the trial. The orientation of the resultant was calculated based on the relative magnitudes of the two components of the drift ratio.

The spread of plasticity was calculated based on the deformations at the lower maximum moment region using two different approaches. In the first alternative the spread of plasticity was defined as the length in which the computed strain exceeded the yield strain of the longitudinal reinforcing bar subjected to the largest tensile demand in the column at the peak relative drift demand. The bars with the highest strain demand in tension and compression were those on opposite ends of the cross section following the orientation of the drift resultant. In the second alternative, the spread of plasticity was calculated as the length in which the curvature exceeded the nominal yield curvature at peak relative drift demand. The curvature was determined along an axis perpendicular to the orientation of the drift resultant.
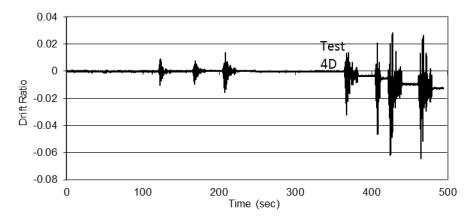

Figure 4. Displacement history recorded at the top of the bridge deck along the transverse direction for all test trials (using sensor DT7).

The computed tensile strain and curvature demands along the column height for the peak drift demand of each test trial are shown in Figs. 5 and 6, respectively. For each trial, the largest tensile strain demand and the largest curvature demand were plotted vs. the peak drift demand in Figs. 7 and 8. Figure 7 shows that as the drift demand increased, the spread of plasticity defined in terms of the tensile strain demand on the reinforcement increased up to a value of 25 in. (635 mm), which was equal to two times of the diameter of the column. This value was recorded during a trial with a peak drift ratio of approximately 2.5%. For trials with larger drift demands, lateral deformation increased due to highly localized damage instead of an increase in the spread of plasticity. This is reflected by Fig. 8, which shows the peak tensile strain demand vs. the peak drift ratio for the trial. As shown in Fig. 8, the peak tensile strain demand continued to increase with the peak drift demand beyond a maximum drift ratio of 2.5%.

The length of the plasticity based on the average curvature showed a slight increase for drift demands greater than 2.5%, with a maximum of approximately 12-in. (305 mm), which is equal to the diameter of the column (Fig. 7).
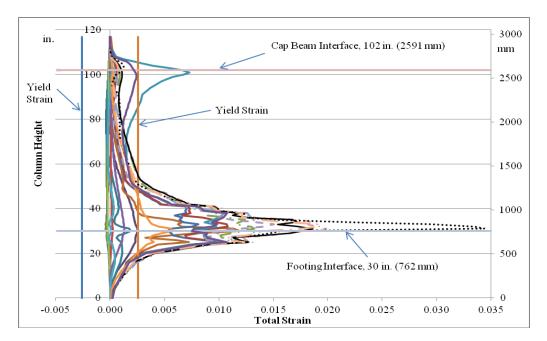
Figure 5. Computed steel strain demand along the longitudinal reinforcing bars (column, cap beam and footing) at each peak relative drift ratio.
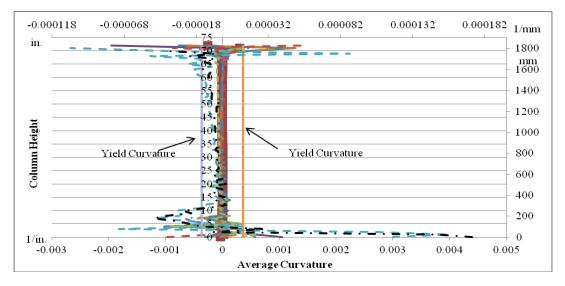

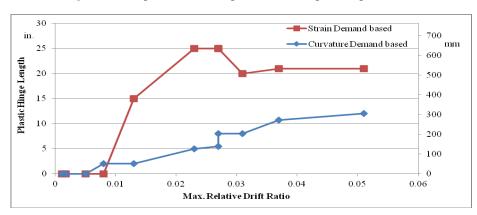**Figure 6.** Computed curvature profiles at each peak displacement.

Figure 7. Plastic hinge length results for each earthquake trial at the peak relative drift ratio.
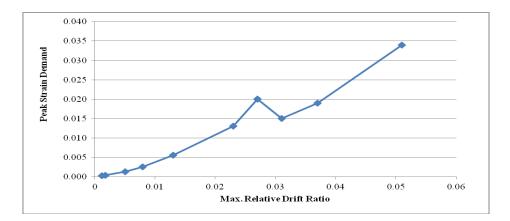
Figure 8. Peak strain demand on the reinforcement at the peak relative drift ratio.

4. SUMMARY AND CONCLUSIONS

A finite element analysis with the optimum model parameters showed that inelastic deformations of the column during entire earthquake trials were concentrated almost entirely at the bottom of the column. Figures 6 and 7 show that in the column member, column response was driven primarily by the deformation of the longitudinal reinforcement. Finite element analyses of the bridge column during eleven earthquake trials indicate that the strain demands in the longitudinal reinforcement exceeded the elastic range in the lowest 25-in. (635-mm) segment of the column, which corresponds to approximately 2 times the diameter of the column. The inelastic strains in the longitudinal bars extended approximately 14 in. (356 mm) or approximately 1 column diameter or 37 longitudinal bar diameters into the joint. Computed curvature demands exceeded the yield curvature over a shorter segment of approximately one column diameter (Figs. 6 and 7). Computed strain demands in the longitudinal reinforcement showed that the highest strain demands occurred over the same bottom 12-in. (305-mm) segment of the column where curvature exceeded the nominal yield curvature, although inelastic deformations extended over a distance 2 times larger. The plastic hinge reached a length of 25 in. (2 times the diameter of the column) when the maximum relative drift ratio was approximately 2.7%. The maximum total tensile strain calculated in the longitudinal bars at a drift ratio of 2.7% was approximately was 0.02, which corresponds to approximately 10 times the yield strain of the steel, and continued to increase with maximum drift demand until reaching a strain of 0.034 (approximately 15 times the yield strain) for a drift ratio of 5.1 %.

Simulation results showed that spread of plasticity calculated in terms of the tensile strain demand in the reinforcement was approximately twice as large as that computed on the basis of the curvature demand. Simulations also showed that the length of the column affected by inelastic deformations in the reinforcement increased up to a drift demand of 2.5%. For ground motions larger drift demands the increase in displacement was accommodated by highly localized deformations in the reinforcement, instead of distributed deformations over the plastic deformation zone.

REFERENCES

Simulia (2009). ABAQUS, Version 6.8-2, http://www.simulia.com.

ASTM (2002). "706/A 706M-01 " Standard Specification for Low-Alloy Steel Deformed and Plain Bars for Concrete Reinforcement," ASTM International, West Conshohocken, Pa.

Bae, S. (2005). "Seismic Performance of Full-Scale Reinforced Concrete Columns", PhD. Dissertation, the University of Texas at Austin, Austin, TX, 311 pp.

Bayrak, O. and Sheikh, S.A. (1997). "High-Strength Concrete Columns under Simulated Earthquake Loading," *ACI Structural Journal* 94:6, 708-722.

Berry, M., Lehman D. E., and Lowes L. N. (2008). "Lumped-Plasticity Models for Performance Simulation of Bridge Columns," *ACI Structural Journal* 105:3, 270-279.

Bhide, S. B., and Collins, M. P. (1987). "Reinforced Concrete Elements in Shear and Tension," Publication No. 87-02, Department of Civil Engineering, University of Toronto, 308 pp.

Collins, M. P., and Mitchell, D. (1987). "Prestressed concrete basics," Canadian Prestressed Concrete Institute, Ottawa.

Dragovich JJ., Lepage A. (2009). "FDE Index for Goodness-of-fit Between Measured and Calculated Response Signals," *Earthquake Engineering and Structural Dynamics* 38:1, 751-1758.

Firat Alemdar Z., Matamoros A., and Browning J. (2011a). "Modeling Surface Deformations and Hinging Regions in Reinforced Concrete Bridge Columns," SL Report No. 11-2, University of Kansas Center for Research, Inc., Lawrence, KS, 60 pp.

Firat Alemdar Z., Browning J., Olafsen J. (2011b). "Photogrammetric Measurements of RC Bridge Column Deformations", *Journal of Engineering Structures*, **33:8**, 2407-2415.

Firat Alemdar Z. (2010). "Evaluation of Plastic Hinge Regions in Reinforced Concrete Bridge Systems," Ph.D. Dissertation, University of Kansas, Lawrence, KS.

Hosoya, H. et al. (1997). "Strain Rate in the Members of Reinforced Concrete Frame Structure During an Earthquake and its Effects. *Journal of Structural and Construction Engineering (Transactions of AIJ)* **499**, 77-83.

Ma, S-Y.M., V.V. Bertero and E.P. Popov. (1976). "Experimental and Analytical Studies of the Hysteretic Behavior of Reinforced Concrete Rectangular and T-Beams," Report No. EERC-76-2, University of California, Berkeley.

Mahin, S.A., Bertero, V. Atalya, M., and Rea, D. (1972). "Rate of Loading Effects on Uncracked and Repaired Reinforced Concrete Members," Report UCB/EERC-72/09, University of California, Berkeley.

Mander J. B. (1983). "Seismic Design of Bridge Piers," PhD. Thesis, University of Canterbury, Christ Church, New Zealand.

Mander J. B., Priestley M. J. N., and Park R. (1984). "Seismic Design of Bridge Piers," Department of Civil Engineering Research Report 84-2, University of Canterbury, 483 pp.

Matamoros A., and Sammarco E. (2010). "Plasticity-Based Nonlinear Finite Element Analysis of Reinforced Concrete Columns with Inadequate Seismic Detailing", *Proceedings of the 9th U.S. National and 10th Canadian Conference on Earthquake Engineering,* Toronto, Canada, July 25-29.

Nelson, R., Saiidi, M., and Zadeh, S. (2007). "Experimental Evaluation of Performance of Conventional Bridge Systems," Center for Civil Engineering Earthquake Research Report No. CCEER-07-04, University of Nevada.

Paulay, T., and Priestley, M. J. N. (1992). "Seismic Design of Reinforced Concrete and Masonry Structures," John Wiley & Sons, Inc.

Priestley M. J. N., and Park, R.. (1987). "Strength and Ductility of Concrete Bridge Columns under Seismic Loading," *ACI Structural J* 84:1. 61-76.

Bentz., E., (2000) "Response-2000. Reinforced Concrete Sectional Analysis using the Modified Compression Field Theory," Version 1.0.5, released August 9th of 2000, http://www.ecf.utoronto.ca/~bentz/r2k.htm.

Sakai, K. and Sheikh, S.A. (1989). "What Do We Know about Confinement in Reinforced Concrete Columns? (A Critical Review of Previous Work and Code Provisions)," *ACI Structural Journal* 86:2, 192-207.

Tanaka, H. and Park, R. (1990). "Effect of Lateral Confining Reinforcement on the Ductile Behavior of Reinforced Concrete Columns," Research Report 90-2, Department of Civil Engineering, University of Canterbury, Christchurch, New Zealand, June, 458 pp.

Vecchio, F. J., and Collins, M. P. (1982). "Response of Reinforced Concrete to in-plane Shear and Normal Stresses," Publ. No. 82-03, Dept. of Civil Engineering, Univ. of Toronto.

Wakabayashi, M. (1986). "Design of Earthquake-Resistant Buildings," New York:McGraw-Hill.

Watson, S. and Park, R. (1994). "Simulated Seismic Load Tests on Reinforced Concrete Columns," *Journal of Structural Engineering, ASCE* 120:6, 1825-1849.